Supplement of Biogeosciences, 19, 4171–4195, 2022
https://doi.org/10.5194/bg-19-4171-2022-supplement

Biogeosciences Open Access EGU

Supplement of

The sensitivity of pCO_2 reconstructions to sampling scales across a Southern Ocean sub-domain: a semi-idealized ocean sampling simulation approach

Laique M. Djeutchouang et al.

Correspondence to: Laique M. Djeutchouang (merlindjeutchouang@gmail.com)

Supplementary Materials

Acronym	Description
FNN	Feed-forward Neural Network
GBM	Gradient Boosting Machines
SAZ	Sub-Antarctic Zone
PFZ	Polar Frontal Zone
NEMO	Nucleus for European Modelling Ocean
PISCES	Pelagic Interactions Scheme for Carbon and Ecosystem Studies
CSIR	Council of Scientific and Industrial Research
SOCCO	Southern Ocean Carbon and Climate Observatory
SOCCOM	Southern Ocean Carbon and Climate Observation Modelling
SOCAT	Surface Ocean CO_2 Atlas
SOSCEx	Southern Ocean Seasonal Cycle Experiment
WG	Waveglider
nUSV	new unmanned surface vehicle
ML	Machine Learning

This supporting information document provides ancillary methodological details and results pertaining to (1) descriptions of the study domain and mode data variables including the motive of the selection of the experimental domain, the characteristics of the NEMO-PISCES model (BIOPERIANT12) data variables of interest and processing, the experimental setting and steps used in the pCO_2 reconstruction; (2) descriptions of the ML regression methods; and (3) additional components on the results and discussion including the model training errors or in-sample uncertainties and biases, and the overall results of the SHIP experiment. Accompanying this supporting information text are four supplementary figures and four supplementary tables.

S1 Descriptions of the study domain and mode data variables

S1.1 Selection of the study domain

According to many studies, the seasonal cycle is the strongest mode of natural variability of carbon dioxide (CO_2) and also the one that most strongly links climate and ocean ecosystems. The seasonal cycle characteristics are largely shaped by higher frequency intra-seasonal modes defining the response modes in physical and biogeochemical components of CO_2 (Mongwe et al., 2016, 2018). For this reason, the Southern Ocean Seasonal Cycle Experiment (SOSCEx) was launched in 2013 - an initiative of the Southern Ocean Carbon-Climate Observatory (SOCCO) which is a research program led by the Council of Scientific and Industrial Research (CSIR). The SOSCEx aimed to explore the nature and links in dynamics and scale sensitivities of atmospheric forcing, CO2 fluxes, and primary production, with a particular focus on the seasonal cycle as a test for the climate sensitivity of earth systems models in respect of the evolution of both atmospheric CO_2 and ocean ecosystems in the 21st century (Swart et al., 2012; Monteiro et al., 2010, 2015). The novel aspect of the third phase (SOSCEx III, 2015-2018) of the project was the integration of a multi-platform approach. This consisted of combining gliders, ships, floats, satellites, and prognostic models in order to explore new questions about the climate sensitivity of CO_2 and ocean ecosystem dynamics. Further, it also investigated how these processes are parameterized in forced ocean models such as the high-resolution (±10km) forced NEMO-PISCES ocean model BIOPERIANT12 (BP12).

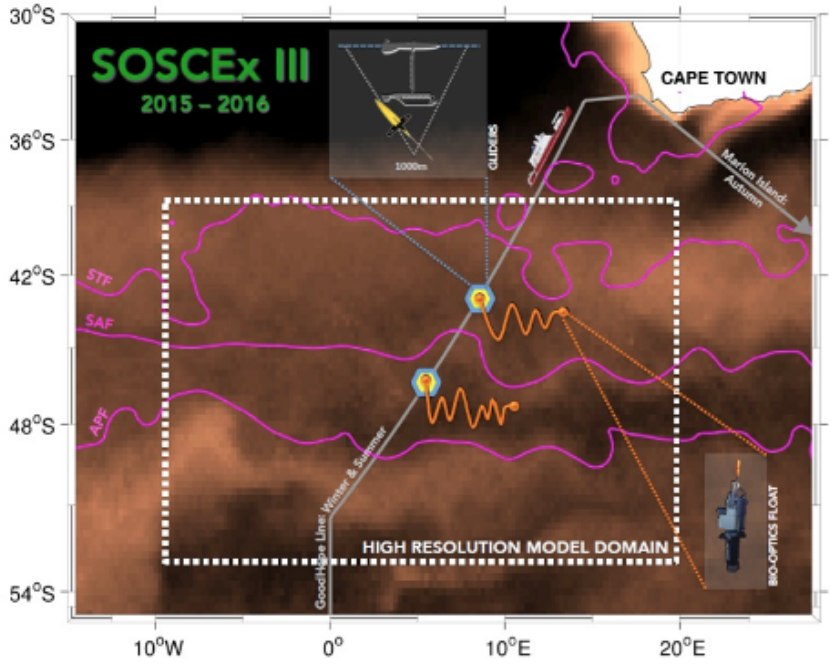

Figure S1: Schematic view of the observing strategy for the beginning of the third phase of the SOSCEx project illustrating the use of multiple SO observing platforms, ships, gliders, floats, and numerical models. The hexagonal patterns (blue-yellow) depict the twined glider deployments; the orange curve shows the Lagrangian float sampling trajectories, while the high-resolution modeling domain is represented with the white dashed line. Magenta lines are the average locations of the oceanic fronts shown as derived

from satellite altimetry data, whereas the underlying shading depicts the mean summer chlorophyll-a concentration in the region with lighter shading=high Chl-a areas. (Source: https://socco.org.za/news/plans-underway-for-soscex-iii/).

S1.2 Data variable characteristics and processing

Here we summarize in Table 1 the data variables of the forced high-resolution (±10km) NEMO-PISCES coupled ocean model BIOPERIANT12, and the processing techniques these variables have to undergo.

Table S1: Summary of the BIOPERIANT12 model variables of interest, and data processing steps applied on feature and target variables.

Variables	Abbreviations	Processing	Date range	Resolutions	
				Space	Time
Air-sea pCO_2 gradient	ΔpCO_2	Model simulations	1 year	1/12º	daily
Atmospheric (atm) pCO_2	pCO_2^{atm}	*In-situ*			
Surface ocean pCO_2	pCO_2 or pCO_2^{ocean}	$pCO_2^{atm} - \Delta pCO_2$			
Sea surface temperature	SST	Model simulations			
Sea surface salinity	SSS	Model simulations			
Mixed layer depth	MLD	Model simulations			
		$\log_{10}$ transformation			
Nano chlorophyll concentration	NChl	Model simulations			
Diatom chlorophyl concentration	DChl	Model simulations			
Chlorophyll-a	Chl-a	NChl + DChl			
Day of the year	J	$\left(\cos\left(j \times \frac{2\pi}{365}\right), \sin\left(j \times \frac{2\pi}{365}\right)\right)$		-	

S1.3 Summary of the experiment

Table S2: Summary of all the 8 semi-idealized ocean system simulation experiments (OSSE-8) that we conducted in this study. The simulated ocean observing platforms (SHIP, FLOAT, WG, and nUSV Saildrone) correspond to their real-world counterparts (ship, carbon-float, Waveglider, and Saildrone) used in the SOCAT project, SOCCOM initiative, and SOCCO program and by Saildrone Inc., respectively. The sampling regimes represent the periods in which the data sampling phase of different experiments occurred according to the temporal scales of the underlying platforms. Note that the observing platforms Waveglider and float have two scenarios each based on the fact that they are deployed either in the north (SAZ) or south (PFZ) of the 10º x 20º experimental domain.

Experiment abbreviations together with their subsequent scenarios (defined by the sampling regimes/strategies) are used in figures and throughout the text.

Ocean Observing Platforms	Sets	Sampling Regimes	Experiments
Ships (SOCAT-like)	SHIP	Summer (smr)	SHIP(smr)
		Summer + Winter (smr+wtr)	SHIP(smr+wtr)
		Autumn + Spring (aut+spr)	SHIP(aut+spr)
Floats (SOCCOM-like)	SHIP + FLOAT	Summer (smr) + One year round	SHIP(smr) + FLOAT(SAZ)
			SHIP(smr) + FLOAT(PFZ)
			SHIP(smr) + FLOAT(SAZ+PFZ)
Wavegliders (SOCCO-like)	SHIP + WG		SHIP(smr) + WG(SAZ)
			SHIP(smr) + WG(PFZ)
Saildrones	SHIP + nUSV		SHIP(smr) + nUSV

S2 Descriptions of the supervised ML regression methods

S2.1 Feed-forward Neural Network

The Feed-forward Neural Network (FNN) is a class of the neuronal network algorithms that is the most commonly used as a non-linear approach in the surface ocean pCO_2 reconstruction community (Bushinsky et al., 2019; Denvil-Sommer et al., 2019; Gloege et al., 2021; Gregor et al., 2019; Gregor and Gruber, 2021; Landschützer et al., 2016; Rödenbeck et al., 2015). Solving the pCO_2 reconstruction problem is within the capability of a single hidden layer of the neural network (Gregor and Gruber, 2021; Landschützer et al., 2013). Thus, we use the Multi-layer Perceptron regressor whose implementation is in the Scikit-learn Python package. The basic principle of this algorithm is summarized in Fig. 2 where a network with random weights is generated similarly to coefficients in the linear regression. Data are passed forward through the network in order to estimate the target values (pCO_2). The difference between estimates and true values is backpropagated through the weights until the targets are met with sufficient accuracy. In our study, we tuned a number of primary hyper-parameters such as the number of hidden layers and weights per layer (see the architecture of the network, e.g., Fig. 2), and the learning rate (α). This tuning

process was achieved with a Bayes-search cross-validation (BayesSearchCV) approach by making use of the Scikit-optimize Python package.

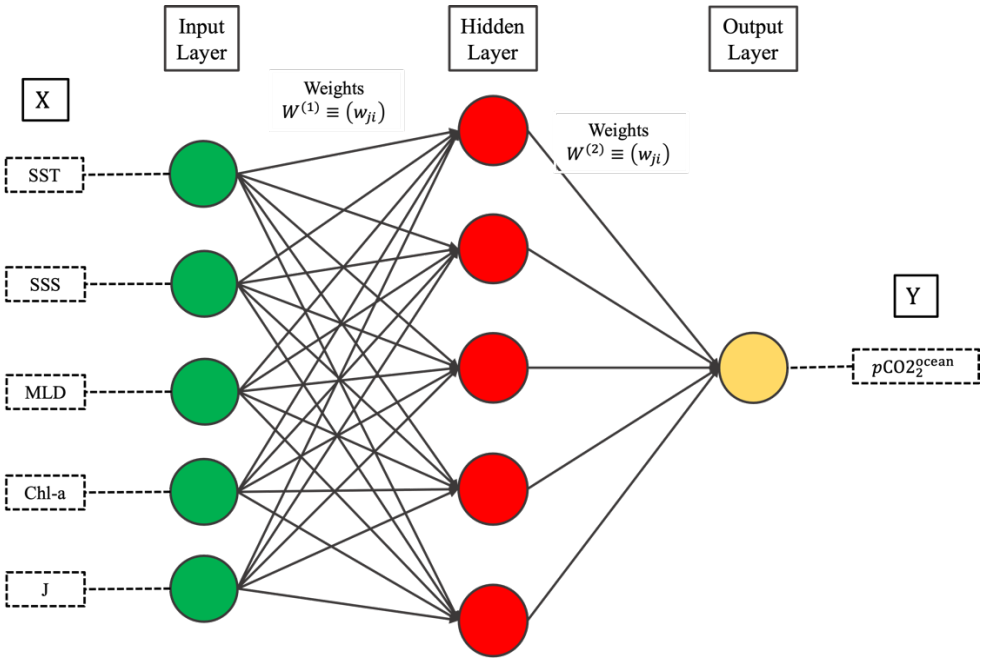

Figure S2: Depiction of a typical example of the architecture or graph of a single hidden layer Multi-layer Perceptron network. X is the array of feature data [SST, SSS, MLD, Chl-a, J] whereas Y is the array of the target variable [pCO_2^{ocean}] as described in Table 1.

S2.2 Gradient Boosting Machines

Gradient Boosting Machines (GBM) is a widely used machine learning (ML) algorithm due to its efficiency, accuracy, and interpretability (Chen and Guestrin, 2016; Gregor et al., 2019; Gregor and Gruber, 2021; Ke et al., 2017). It is a variant of the Gradient Boosting Decision Tree (GBDT) learning frameworks. GBM produces a prediction model in the form of an ensemble of weak prediction models typically called decision tree learners that increase the efficiency of the model and reduce memory usage during the training. It builds these multiple weak learners in a stage-wise or sequential fashion and generalizes them by allowing optimization of an arbitrary differentiable loss function (Friedman, 2001; Ke et al., 2017). This can be known as aggregative learning, where in each stage algorithm improves what is learned. Although GBM has been proven to deal well with imbalanced or sparse datasets (Ke et al., 2017)), it is more likely to overfit the training data because of the model's potential for high complexity (Frery et al., 2017). Thus, tuning GBM hyper-parameters to prevent overfitting is very important. In our study, the following hyper-parameters were tuned: number of trees or leaves, depth of the trees, learning rate, number

of estimators, and boosting type. We use the LightGBM and Scikit-optimize Python packages for our implementation of GBM and optimization/tuning of hyper-parameters through the BayesSearchCV module, respectively.

S2.3 Surface ocean pCO_2 reconstruction steps

Two commonly used reconstruction techniques (Landschutzer et al, 2016; Gregor et al., 2019) that also motivated the choice of two machine learning methods above (FNN and GBM) both adopt a two-step ML approach in which the first step consists of clustering the reconstruction domain whereas the second step applies ML regression mapping in each cluster generated. At large-scale reconstructions such as the Southern Ocean as a whole, this clustering step is necessary to overcome the spatial and temporal limitations of observations. Fig. S3 illustrates the Southern Ocean Fay and McKinley (2014) biomes, one of the clustering methods used by Gregor et al. (2019). This helps to understand the motive of skipping the clustering step in this study. Fig. S3a shows that the clustering step was not necessary given the size of the study domain, which is very smaller compared to the clusters. The study domain (black box, Fig. S3a) is roughly 50% STSS/SPSS (Fig. S3b).

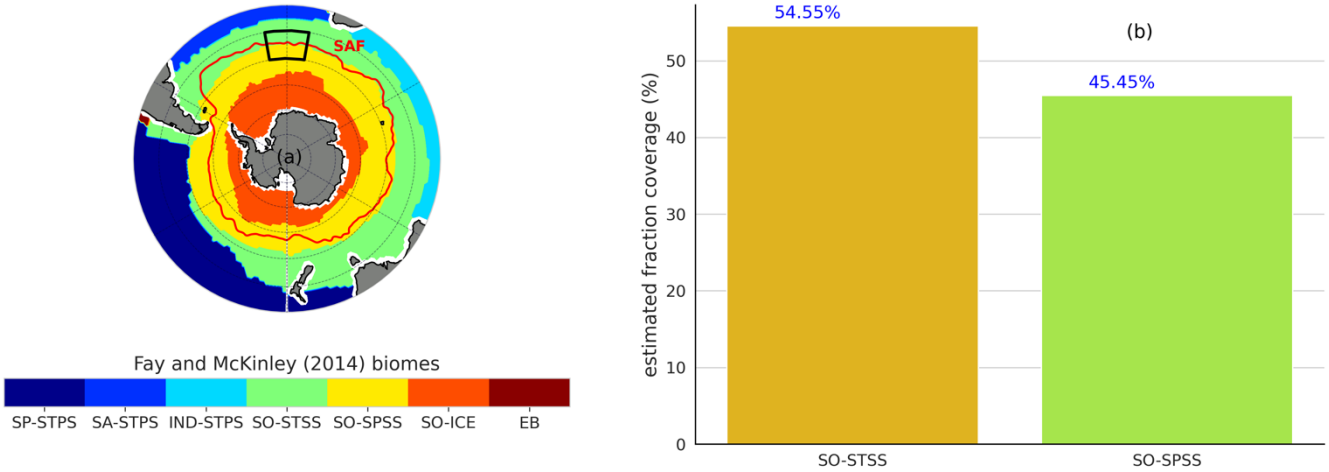

Figure S3: Panel (a) is the Southern Ocean regions or biomes (Fay and McKinley, 2014) as extended and used in Gregor et al. (2019) on which are added the Sub-Antarctic Front (SAF) (red line) dividing the study domain (black box) into the Sub-Antarctic Zone (SAZ) and Polar Frontal Zone (PFZ) which are relatively the two most sampled regions of the Southern Ocean; and panel (b) show the fraction coverage estimates (%) of the two most sampled regions: STSS and SPSS biomes relatively to the area of our box. EB biome stands for Eastern Boundaries (Gregor et al., 2019). For other biome abbreviations (below the colour bar), see Fay and McKinley (2014).

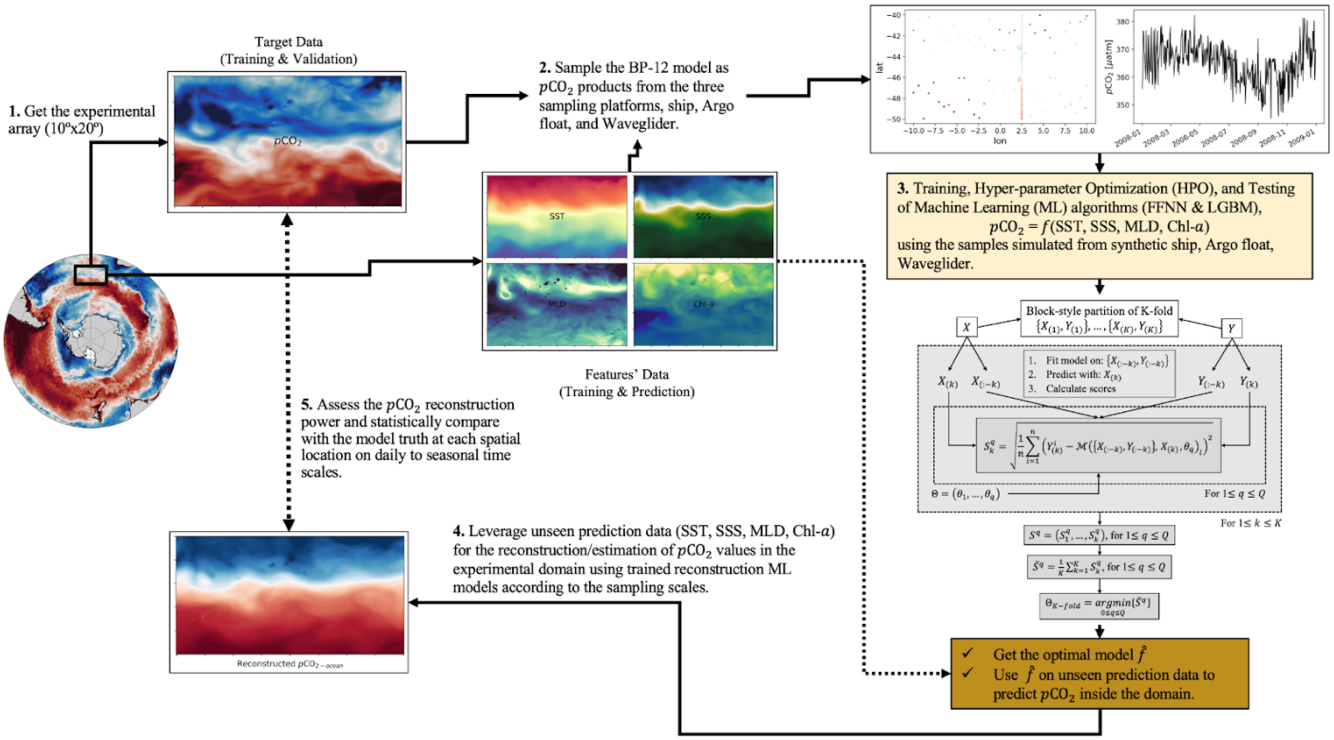

Figure S4: Schematic flow diagram showing the key steps required to reconstruct the surface ocean pCO_2 in the full experimental domain.

S3 Results and Discussion

S3.1 ML regression in-sample scores for individual methods

In-sample scores correspond to ML regression scores calculated from all the training data points. This allowed for controlling the overfitting of the methods during the training. For instance, by focusing on the root mean square errors (RMSEs) and the mean bias errors (MBEs) or simply biases reported in Table 3, the nuanced differences between the two ML regression methods FNN and GBM show that the GBM method was likely susceptible to overfitting on training data compared to FNN method.

Table S3: Various in-sample errors (i.e., errors calculated from all the training points) for empirical estimates of the surface ocean pCO2 for different experiments we run. The configuration of these experiments is presented in Table 1 and clearly described in Section 2.3.2. The machine learning regression metrics we used to report this in-sample error are abbreviated as follows: RMSE is the root mean square error; MAE is the mean absolute error; MBE or Bias is the mean average error.

Sets	Sampling Regimes	Experiments	Algorithms	RMSE (µatm)	MAE (µatm)	MBE (µatm)
SHIP		SHIP(smr)	FNN	4.07	3.39	0.14

	Summer (smr)		GBM	0.84	0.65	0.01
	Summer + Winter (smr+wtr)	SHIP(smr+wtr)	FNN	5.19	4.09	-0.51
			GBM	1.41	1.07	0.02
	Autumn + Spring (aut+spr)	SHIP(aut+spr)	FNN	3.78	3.05	0.19
			GBM	2.25	1.75	0.08
SHIP + FLOAT	Summer (smr) + One year round	SHIP(smr) + FLOAT(SAZ)	FNN	6.21	5.06	0.21
			GBM	1.49	1.12	0.06
		SHIP(smr) + FLOAT(PFZ)	FNN	5.11	4.17	0.08
			GBM	0.85	0.64	0.02
		SHIP(smr) + FLOAT(SAZ+PFZ)	FNN	8.76	7.52	-2.01
			GBM	1.49	1.12	0.06
SHIP + WG		SHIP(smr) + WG(SAZ)	FNN	4.12	2.92	0.38
			GBM	0.54	0.35	0.01
		SHIP(smr) + WG(PFZ)	FNN	2.27	1.65	-0.12
			GBM	0.08	0.05	0.02
SHIP + nUSV		SHIP(smr) + nUSV	FNN	5.39	4.29	-0.11
			GBM	2.55	1.98	-0.03

S3.2 Hyper-parameter report after tuning

Both machine learning algorithms (FNN and GBM) involved in the two-member ensemble method used in this study come with many hyper-parameters that are simply parameters whose values are determined by the training but need to be provided for the training or fitting of an algorithm. We made use of K-fold cross-validation technique combined with Bayesian optimization to achieve this process. For the reproducibility purpose, the optimal values of hyper-parameters reported at the end of the training are present in Table S4.

Table S4: Final values used after tuning the hyper-parameters in the following experiments: SHIP(smr), SHIP(smr+wtr), SHIP(aut+spr), SHIP(smr) + WG(SAZ), and SHIP(smr) + WG(PFZ).

Algorithms	**Hyper-parameters**	**Final value used per experiment**				
		SHIP (smr)	SHIP (smr+wtr)	SHIP (aut+spr)	SHIP(smr) + WG(SAZ)	SHIP(smr)+ WG(PFZ)
GBM	Boosting type	gbdt	gbdt	gbdt	gbdt	goss
	No. of estimators	128	256	260	185	150

	Learning rate	0.005	0.1	0.0408	0.0366	0.0409
	Max depth	8	32	16	16	8
	No. leaves	32	64	64	128	160
	Min data leaf	50				
FNN	No. of hidden layers	1				
	Hidden layer size	32	115	128	128	64
	Learning rate	Adaptive (0.001)				
	Alpha	0.0001	0.0143	0.1	0.0001	0.0145
	Activation function	relu				
	Optimizer/Solver	adam				
	Batch size	auto				

Table S5: Final values used after tuning the hyper-parameters in the following experiments: SHIP(smr) + FLOAT(SAZ), SHIP(smr) + FLOAT(PFZ), SHIP(smr) + FLOAT(SAZ+PFZ) , and SHIP(smr) + nUSV.

Algorithms	**Hyper-parameters**	**Final value used per experiment**			
		SHIP(smr) + FLOAT(SAZ)	SHIP(smr) + FLOAT(PFZ)	SHIP(smr) + FLOAT(SAZ+PFZ)	SHIP(smr) + nUSV
GBM	Boosting type	goss	gbdt	goss	goss
	No. of estimators	230	220	250	260
	Learning rate	0.0503	0.0145	0.0455	0.0258
	Max depth	32	32	16	32
	No. leaves	128	160	128	256
	Min data leaf	50			
FNN	No. of hidden layers	1			
	Hidden layer size	128	64	128	128
	Learning rate	Adaptive (0.001)			
	Alpha	0.0001	0.0065	0.0002	0.0059
	Activation function	relu			
	Optimizer/Solver	adam			
	Batch size	auto			

S3.3 Overall results from the SHIP experiment

S3.3.1 The spatial and seasonal cycle anomalies

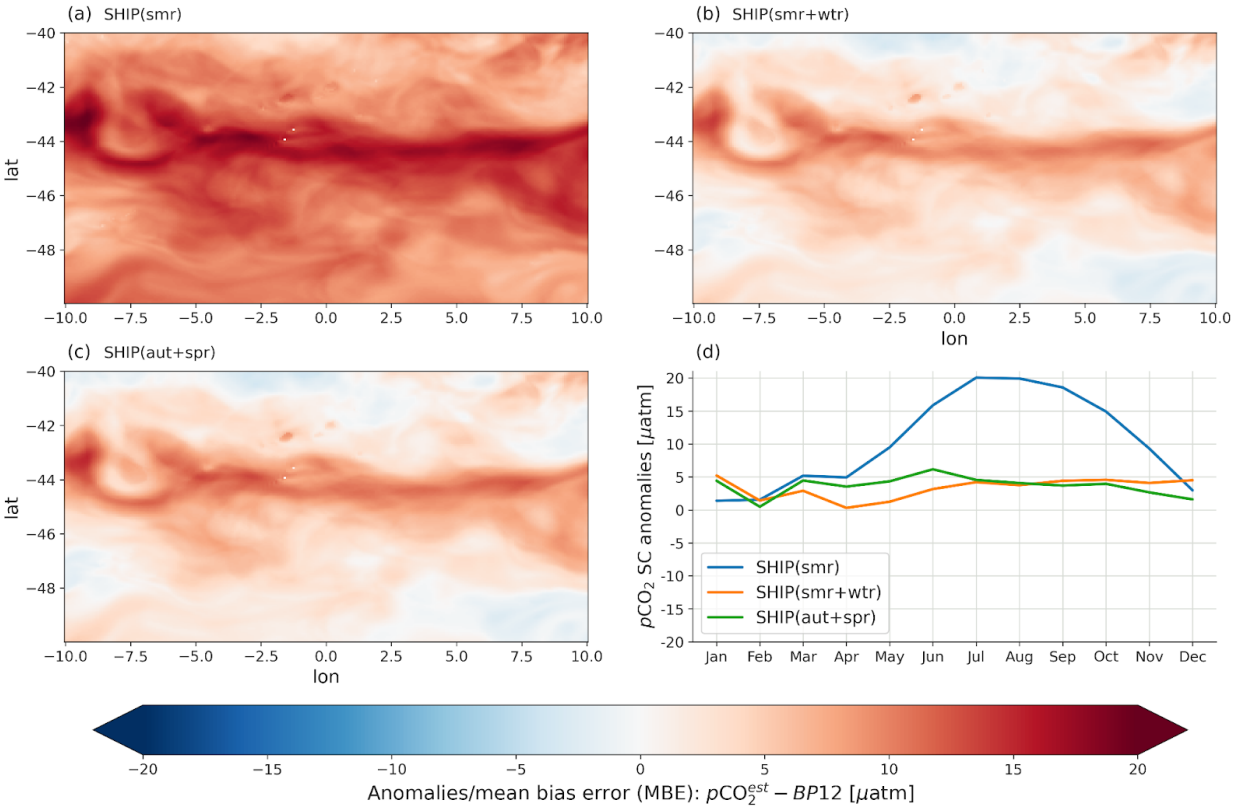

Figure S5: Reconstruction anomalies for the idealized SHIP experiment where the idealized ship sampled the domain according to the three sampling regimes/scenarios, summer (smr), summer + winter (smr+wtr), and autumn + spring (aut+spr). Panels (a), (b) and (c) show the maps of the reconstruction anomalies based these three sampling regimes, hence the three experiments SHIP(smr), SHIP(smr+wtr), and SHIP(aut+spr) respectively; panel (d) shows the anomalies of the mean seasonal cycle (SC) reconstruction based on these three sampling regimes; that is, SHIP(smr), SHIP(smr+wtr) , and SHIP(aut+spr).

S3.3.2 Reconstruction skills for the SHIP experiment

Table S6: ML regression modelling scores of the ensemble average (ML2) for the SHIP set of experiments: SHIP(smr) for summer sampling, SHIP(smr+wtr) for summer and winter sampling, and SHIP(aut+spr) for autumn and spring sampling. The configuration of this set of experiments is presented in Table S2. The first column of the table is the experimental set and the second one corresponds to the considered experiments. The statistical metrics used to assess ML2 for this set of experiments are abbreviated as follows: RMSE is the root mean square error; MAE is the mean absolute error; MBE or Bias is the mean average error, and r is the Pearson's

correlation coefficient between the reconstructed and BP12 model truth pCO_2. Values in the table are significantly different from the mean for the corresponding column (with a 95% confidence level or p-value < 0.05 for the two-tailed Z-test).

Sets	Experiments	RMSE (µatm)	MAE (µatm)	MBE (µatm)	r
SHIP	SHIP(smr)	13.79	11.51	10.52	0.36
	SHIP(smr+wtr)	6.8	5.29	3.18	0.73
	SHIP(aut+spr)	7.07	5.5	3.57	0.72

S3.4 Approximation of the monetary cost of nUSV to the full Southern Ocean

To estimate the sampling density of nUSV in the Southern Ocean, a subset of Sutton et al. (2021)-USV dataset was created within the study sub-domain in order to get its original sampling tracks (Fig. S6). We found that the Sutton et al. (2021)-USV would take ~16 days to cover our 20ºW-E domain, which corresponds to 16days * 24hrs = 384 hourly samples. Longitudinally, on the other hand, the Southern Ocean is equal to 360º/20º = 18 times our 20ºW-E domain. This means that it would take about 18 nUSV Saildrones to sample the full Southern Ocean. Further, based on a Science Magazine News by Paul Voosen (March 8, 2018), Saildrone Inc charges about $2500 a day per nUSV to collect ocean data, whereas ship time can cost about $30,000 or more per day. According to our estimation above, nUSV would sample hourly the sub-domain in about 16 days. Therefore, using the nUSV, sampling one circumpolar frontal region of the Southern Ocean with a density similar to that of our experiment would cost about 18*16 * $2 500 = $720 000. This is the upper end of the estimate.

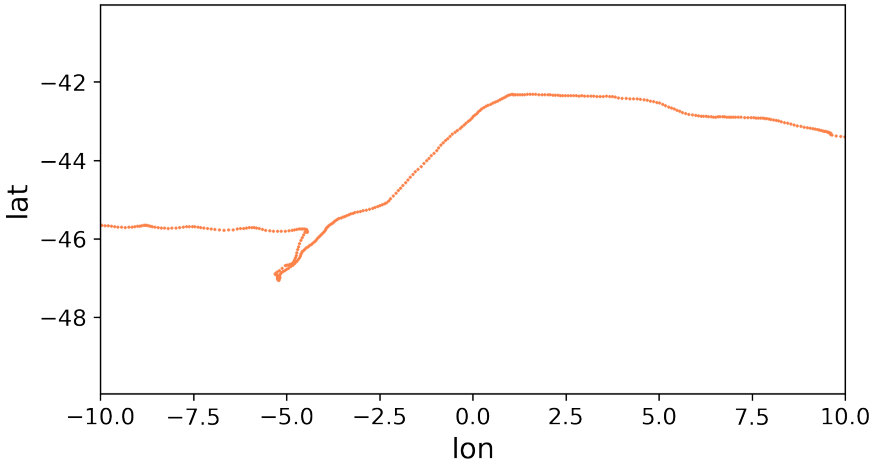

Figure S6: Sampling tracks of Sutton et al. (2021) USV inside the study domain.

S3.5 Additional details on the importance of synoptic scales in sampling

More coordinated deployments of floats are necessary to resolve, for example, the intra-seasonal variability that nUSV and WGs were able to resolve. The resolving of this synoptic scale by WG and nUSV systems is likely due to their high sampling frequency, which would mean that sampling surface ocean CO_2 at the correct interval remains critical. In addition, based on the sampling period sensitivity analysis (Fig. S7), Monteiro et al. (2015) showed that to achieve the 10% uncertainty threshold in the Southern Ocean as discussed in Lenton et al. (2006), a sampling period of 1-3 days is necessary for areas of high EKE and elevated sub-seasonal dynamics like that of the study domain. Thus, having a perfect knowledge of how we need to sample, one can get an estimate of the sensitivity of pCO_2 to various sampling frequencies.

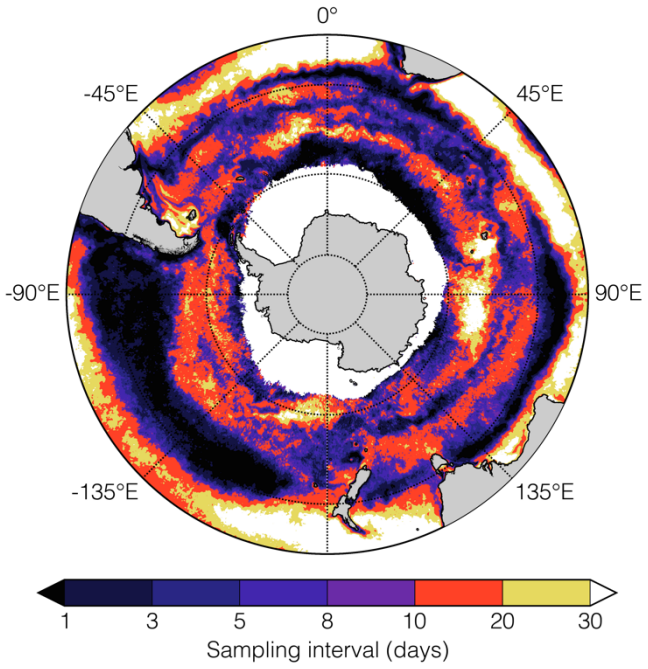

Figure S7: A map from Monteiro et al. (2015) showing a mean for the adaptive sampling interval (in days) required to achieve the 10% uncertainty threshold in the Southern Ocean as discussed in Lenton et al. (2006).

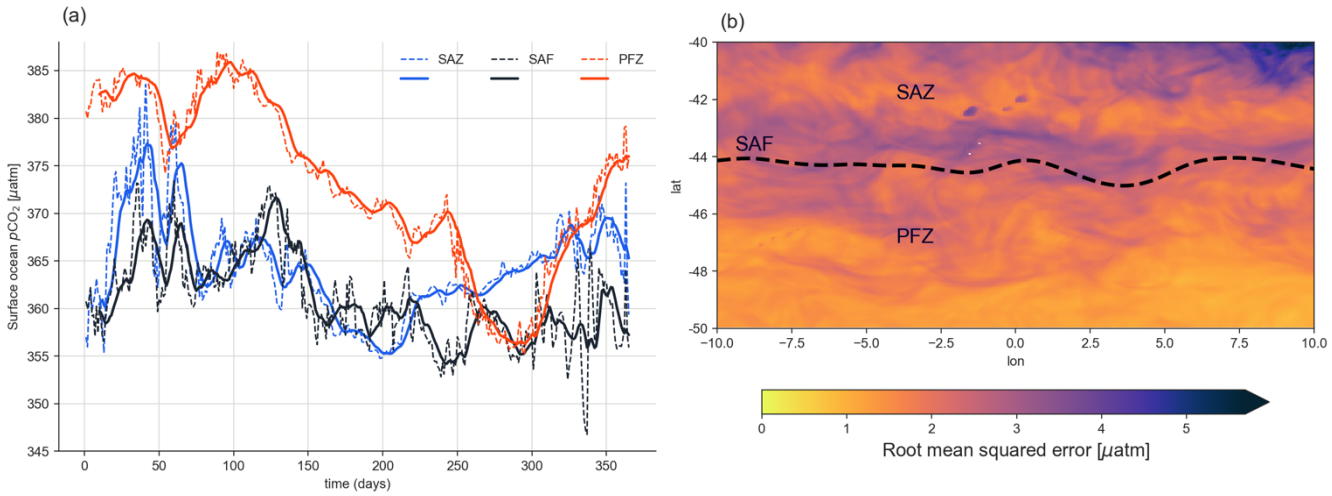

Figure S8: Panel (a) shows one-year time series plots (dashed lines) of the variability of pCO_2 at single-model grid cells on the SHIP line (2.5°E) and in solid lines the 10-day rolling mean (i.e., low-pass filtered pCO_2 where the duration is set to 10 days). We used the following single model grid cells: 42°S, 2.5°E in the Sub-Antarctic Zone (SAZ); 44°S, 2.5°E on the Sub-Antarctic Front (SAF); and 47°S, 2.5°E in the Polar Frontal Zone (PFZ). Panel (b) shows the RMSE map of the difference of the 10-day rolling mean from the daily model pCO_2 in the study domain divided by the SAF (black dashed line, Fig. S8b) into two sub-domains: the SAZ and the PFZ. This RMSE gives us a statistical understanding of what the uncertainty might be if we sampled at a 10-day rate.

References

Bushinsky, S. M., Landschützer, P., Rödenbeck, C., Gray, A. R., Baker, D., Mazloff, M. R., Resplandy, L., Johnson, K. S., and Sarmiento, J. L.: Reassessing Southern Ocean Air-Sea CO2 Flux Estimates With the Addition of Biogeochemical Float Observations, 33, 1370–1388, https://doi.org/10.1029/2019GB006176, 2019.

Chen, T. and Guestrin, C.: XGBoost: A Scalable Tree Boosting System, in: Proceedings of the 22nd ACM SIGKDD International Conference on Knowledge Discovery and Data Mining, 785–794, https://doi.org/10.1145/2939672.2939785, 2016.

Denvil-Sommer, A., Gehlen, M., Vrac, M., and Mejia, C.: LSCE-FFNN-v1: A two-step neural network model for the reconstruction of surface ocean pCO2 over the global ocean, 12, 2091–2105, https://doi.org/10.5194/GMD-12-2091-2019, 2019.

Frery, J., Habrard, A., Sebban, M., Caelen, O., and He-Guelton, L.: Efficient Top Rank Optimization with Gradient Boosting for Supervised Anomaly Detection BT - Machine Learning and Knowledge Discovery in Databases, 20–35, 2017.

Friedman, J. H.: Greedy function approximation: A gradient boosting machine, 29, 1189–1232, https://doi.org/10.1214/aos/1013203451, 2001.

Gloege, L., McKinley, G. A., Landschützer, P., Fay, A. R., Frölicher, T. L., Fyfe, J. C., Ilyina, T., Jones, S., Lovenduski, N. S., Rodgers, K. B., Schlunegger, S., and Takano, Y.: Quantifying Errors in Observationally Based Estimates of Ocean Carbon Sink Variability, 35, e2020GB006788, https://doi.org/10.1029/2020GB006788, 2021.

Gregor, L. and Gruber, N.: OceanSODA-ETHZ: A global gridded data set of the surface ocean carbonate system for seasonal to decadal studies of ocean acidification, 13, 777–808, https://doi.org/10.5194/ESSD-13-777-2021, 2021.

Gregor, L., Lebehot, A. D., Kok, S., and Scheel Monteiro, P. M.: A comparative assessment of the uncertainties of global surface ocean CO2 estimates using a machine-learning ensemble (CSIR-ML6 version 2019a)-Have we hit the wall?, 12, 5113–5136, https://doi.org/10.5194/gmd-12-5113-2019, 2019.

Ke, G., Meng, Q., Finley, T., Wang, T., Chen, W., Ma, W., Ye, Q., and Liu, T. Y.: LightGBM: A highly efficient gradient boosting decision tree, 2017-Decem, 3147–3155, 2017.

Landschützer, P., Gruber, N., Bakker, D. C. E., Schuster, U., Nakaoka, S., Payne, M. R., Sasse, T. P., and Zeng, J.: A neural network-based estimate of the seasonal to inter-annual variability of the Atlantic Ocean carbon sink, 10, 7793–7815, https://doi.org/10.5194/bg-10-7793-2013, 2013.

Landschützer, P., Gruber, N., and Bakker, D. C. E. E.: Decadal variations and trends of the global ocean carbon sink, 30, 1396–1417, https://doi.org/10.1002/2015GB005359, 2016.

Mongwe, N. P., Chang, N., and Monteiro, P. M. S.: The seasonal cycle as a mode to diagnose biases in modelled CO2 fluxes in the Southern Ocean, 106, 90–103, https://doi.org/10.1016/j.ocemod.2016.09.006, 2016.

Mongwe, N. P., Vichi, M., and Monteiro, P. M. S.: The seasonal cycle of <i>p</i>CO₂ and CO₂ fluxes in the Southern Ocean: diagnosing anomalies in CMIP5 Earth system models, 15, 2851–2872, https://doi.org/10.5194/bg-15-2851-2018, 2018.

Monteiro, P. M. S., Schuster, U., Hood, M., Lenton, A., Metzl, N., Olsen, A., Rogers, K., Sabine, C., Takahashi, T., Tilbrook, B., Yoder, J., Wanninkhof, R., and Watson, A. J.: A Global Sea Surface Carbon Observing System: Assessment of Changing Sea Surface CO2 and Air-Sea CO2 Fluxes, 702–714, https://doi.org/10.5270/OCEANOBS09.CWP.64, 2010.

Monteiro, P. M. S., Gregor, L., Lévy, M., Maenner, S., Sabine, C. L., and Swart, S.: Intraseasonal variability linked to sampling alias in air-sea CO2 fluxes in the Southern Ocean, 42, 8507–8514, https://doi.org/10.1002/2015GL066009, 2015.

Rödenbeck, C., Bakker, D. C. E., Gruber, N., Iida, Y., Jacobson, A. R., Jones, S., Landschützer, P., Metzl, N., Nakaoka, S., Olsen, A., Park, G. H., Peylin, P., Rodgers, K. B., Sasse, T. P., Schuster, U., Shutler, J. D., Valsala, V., Wanninkhof, R., and Zeng, J.: Data-based estimates of the ocean carbon sink variability - First results of the Surface Ocean pCO2Mapping intercomparison (SOCOM), 12, 14049–14104, https://doi.org/10.5194/bgd-12-14049-2015, 2015.

Swart, S., Chang, N., Fauchereau, N., Joubert, W., Lucas, M., Mtshali, T., Roychoudhury, A., Tagliabue, A., Thomalla, S., Waldron, H., and Monteiro, P. M. S.: Southern Ocean Seasonal Cycle Experiment 2012: Seasonal scale climate and carbon cycle links, 108, 3–5, https://doi.org/10.4102/sajs.v108i3/4.1089, 2012.